Proceedings of ASME Turbo Expo 2011
GT2011
June 6-10, 2011, Vancouver, British Columbia, Canada

GT2011-46401

A STUDY OF HEAT TRANSFER AUGMENTATION FOR RECUPERATIVE HEAT EXCHANGERS: COMPARISON BETWEEN THREE DIMPLE GEOMETRIES

Michelle I. Valentino, Lucky V. Tran, Mark Ricklick, J.S. Kapat
Center for Advanced Turbines and Energy Research
Laboratory for Turbine Aerodynamics, Heat Transfer, and Durability
University of Central Florida Orlando, FL USA

ABSTRACT

This study presents an investigation of the heat transfer augmentation for the purpose of obtaining high effectiveness recuperative heat exchangers for regeneration. The focus of the present work is in the fully developed portion of a 2:1 aspect ratio rectangular channel characterized by dimples applied to one wall at channel Reynolds numbers of 10,000, 18,000, 27,000, and 36,000. The dimples are applied in a staggered-row, racetrack configuration. In this study, a segmented copper test section was embedded with insulated dimples in order to minimize (to a negligible level) the heat transfer within the dimpled feature. The insulated material used to create a dimpled geometry isolates the heat transfer within the dimple cavity from the heat transfer augmentation on the surrounding smooth walls promoted by the flow disturbances induced by the dimple. Results for three different geometries are presented, a small dimple feature, a large dimple, and a double dimple. The results of this study indicate that there is significant heat transfer augmentation even on the non-featured portion of the channel wall. Overall heat transfer augmentations for the small dimples are between 13-27%, large dimples between 33-54%, and double dimples between 22-39%, with highest heat transfer augmentation at the lowest Reynolds number for all three dimple geometries tested.

INTRODUCTION

Advancements in heat transfer technology for recuperative heat exchangers in small gas turbines, or microturbines, are increasingly being investigated to improve cycle efficiency. Recuperators, which are used to pre-heat air before entering the combustion section, are outfitted with transport enhancing geometries to improve the heat transfer performance. A variety of geometries have been introduced as transport enhancements for recuperative heat exchangers; the added roughness of the surface geometries break up the laminar sub-layer of the channel flow and promote mixing and secondary flows throughout the channel. Transport enhancements such as ribs, pin fins, swirl chambers, scales, and dimples have all been reviewed for contribution to mixing and secondary flows.

The use of transport enhancers to achieve a higher heat transfer performance is seen in several applications including recuperative heat exchangers, electronic cooling, and gas turbine cooling. One key concern when applying these features is how to enhance the heat transfer without a corresponding high increase in pressure penalty, especially important for recuperative heat exchangers. Dimpled features are known for their ability to improve heat transfer without contributing to a high loss in pressure.

The application of dimples can be seen as early as 1966, where Snedeker and Donaldson carried out an experimental study on flow inside of a hemispherical cavity [1]. Although this had more aerodynamic applications, the idea of using a dimpled surface to promote heat transfer followed with a further characterization of the flow behavior by Murzin et al. [2]. Belen'kiy et al. used a staggered array of surface indentions to improve heat transfer in a shell and tube heat exchanger [3]. Terekhov et al. provided the first quantitative measurements of flow inside of a dimple with laser diagnostics [4]. Other designs of the dimples included a tear-drop shape; this design was experimented and compared with the hemispherical concavity using transient TLC by Chyu et al. [5]. Moon et al. studied turbulent heat transfer measurements on a wall with concave and cylindrical dimples in a square channel [6].

Dimpled surfaces are becoming more prevalent in current studies because of their ability to promote mixing of the flow without creating high pressure losses through the channel. A concavity approach for use in compact heat exchangers was studied by Chyu et al. [7]. The effect of channel height on heat transfer and friction in dimpled cooling passages was studied by Moon et al. [8]. Research into the secondary flows or vortices created by the dimple feature was studied using smoke visualization and Mahmood et al. studied the spanwise-normal distribution of time averaged velocity and pressure using Kiel and static pressure probe measurements over a staggered array of dimples on a flat plate [9]. This study showed a primary vortex pair existing along the longitudinal line of symmetry as well as two additional secondary vortices formed periodically on each side of the primary vortex pair. Following this study,

Mahmood and Ligrani studied the effect of aspect ratio, temperature ratio, and Reynolds number on the flow structure and heat transfer in a dimpled array [10]. Ligrani et al. conducted similar experiements as in [9,10], with additional five-hole probe measurements as well as constant temperature anemometry for longitudinal velocity fluctuations [11]. Won et al. compared flow structures above a dimpled surface with similar measurement techniques [12]. Burgess et al. discussed Nusselt number behavior on deep dimpled surfaces [13]; Burgess and Ligrani studied the effect of dimple depth on Nusselt numbers and friction factors for an array of dimples, concluding that the highest heat transfer augmentations were found at the downstream dimple edge and the flat surface just downstream of the dimple [14,15]. Results of numerical solutions of turbulent convective heat transfer with a single spherical dimple were then presented by Isaev et al. [16]. Applying dimples to rotating machinery, Griffith et al. studied the effects of rotation of a rectangular channel with dimples applied to two walls [17].

Zhao compared the friction coefficient in a smooth walled channel to a dimpled channel, finding the difference to be within the range of experimental uncertainty [18]. Borisov et al. presented a "banked" dimple and protrusion design and reported heat transfer and pressure loss through the channel [19]. Borisov et al. also studied heat transfer and pressure losses in a narrow dimpled-protrusion channel for application in a recuperator core [20]. Effects of combined dimpled/protrusion walls on thermal performance inside a channel at low Reynolds numbers were then examined by Hwang et al. [21]. Leinhart et al. performed both numerical and experimental analysis of turbulent flow over a dimpled surface to determine the effect on skin-friction drag [22]. Recent studies varying dimensions or overall shape of the dimple to review the effects on heat transfer and friction augmentation include Isaev et al. who studied the dimple depth on these effects [23]. Leontiev et al. also conducted a numerical study of turbulent air flow and heat transfer for a narrow channel [24]; the channel height was varied while maintaining the dimple shape, and then the dimple diameter was varied while maintaining a constant channel cross section.

Previous work, by Elyyan, studied both dimpled surface features as well as a split dimple-fin configuration [25,26]. As an alternative to traditional recuperators, a microchannel heat exchanger using polymer derived ceramics was studied by Carman et al. [27]. Stacking narrow microchannels for compact heat exchangers, low aspect ratio channels as studied in this paper, can increase the surface area density in a given volume of the recuperator core.

Different fabrication methods are used for manufacturing recuperative heat exchangers; a common method, the stamping method, often results in one side being dimpled and the other with protrusion shapes (see Fig. 1). The optimization of these heat exchangers requires a detailed understanding of the interactions between the dimples and protrusions. However, before the combined interactions between these two features

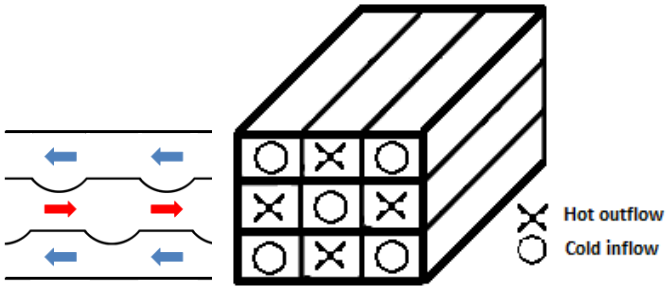

Figure 1: Dimple-Protrusion Surface for Counterflow Compact HX

can be fully understood, further insight to the nature of the secondary flows caused by the dimple alone is required, which is an objective of this paper.

Slabaugh et al. studied altering the dimple shape or footprint, looking at two dimple footprint diameters as well as a double-dimpled feature and the effect the dimples produce on the side walls of a small aspect ratio channel (AR=2) using a modular copper block test section implemented with thermocouples in [28]. This study concluded that the double dimple shape produced a higher heat transfer augmentation at a much lower cost of pressure drop in the channel. Slabaugh et al. then performed transient TLC measurements on an upscaled acrylic channel to obtain local heat transfer coefficients on all four walls of the channel [29]. The double-dimple shape was further reviewed by Slabaugh using numerical modeling through LES [30].

The change in shape from a single dimple to a double dimple creates an increase in the streamwise length. The double dimple incorporates two spherical dimples into one feature, creating a ridge between the upstream and downstream dimple that does not exist in a single dimple feature. The presence of this ridge may disrupt the flow and reduce the size of the recirculation zone. In addition, the increased streamwise length of the feature allows for the flow to enter and exit the dimple more gradually (no large angle ejection) and has a better reattachment than seen in the single dimple (see Fig. 2). A known issue with dimples is that these modified surfaces in gas turbines and heat exchangers are susceptible to fouling. Insulating the dimple allows some insight into minor fouling within the dimple cavity and the effect on heat transfer augmentation of the channel. However, the problem of fouling is beyond the scope of the current experiment, its effects on a double dimple are expected to be similar to the traditional single dimple.

The present study differs from previous experiments by creating a confined dimple space with top and side walls and observing the effects on heat tranfer for all four walls and comparing quantitatively the heat transfer augmentation effects on the dimpled and non-dimpled portion of the bottom wall for three different dimple geometries. A different method of investigation is used, copper blocks with thermocouples rather than TLC or IR. The transient TLC method in particular, which was widely employed in most previous studies on dimpled heat

transfer, inherently assumes a purely one-dimensional semi-infinite solid. In reality, the transient conduction process is three dimensional and the effect of lateral conduction must be taken into account if accurate results are to be obtained, especially around the curved surface and sharp edges of the dimple feature. In the results reported by Slabaugh et al. [28], a clear bias in improved heat transfer was obtained with the transient TLC method as compared to copper blocks with thermocouples, which was well beyond the experimental uncertainty of both experiments. Griffith et al. point out the large variations in heat transfer enhancement results (10-20%) depending on what measurement and method of analysis is being used [17]. The high thermal conductivity copper block with embedded thermocouples used in this study represents a true, spatially-averaged Nusselt number and captures any effects from the other walls (the smooth top and side walls). Potential side and top wall effects would not be included in the averages of others [9-15], where values were averaged over only one or a few dimple periods at the center of a vast array of dimples.

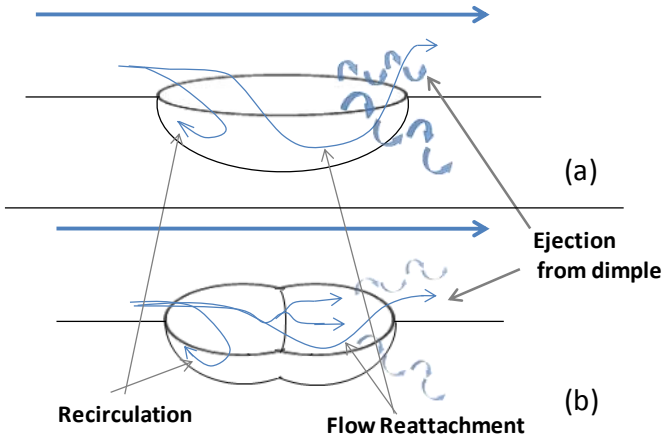

Figure 2: Flow Structures in a (a) Single Dimple (b) Double Dimple

NOMENCLATURE

Roman Symbols

A	Surface Area
Bi	Biot Number
c	Specific Heat Capacity
d	Dimple Footprint Diameter
D	Diameter
DD	Double Dimple
t	Thickness of cork insulation
h	Convective Heat Transfer Coefficient
H	Channel Height
k	Thermal Conductivity
Nu	Nusselt Number
P	Pitch of Dimple Array
Pr	Prandtl Number
Q”	Surface Heat Flux
Q_{added}	Heat Input to the Flow
Q_{input}	Power Input
$Q_{lateral}$	Lateral Heat Conduction
Q_{loss}	Ambient Heat Loss
Re	Reynolds Number
S	Longitudinal Dimple Pitch
SD	Single Dimple
T	Temperature
V	Voltage
W	Channel Width

Greek Symbols

α	Thermal Diffusivity
δ	Dimple Depth
υ	Kinematic Viscosity
ρ	Density
μ	Fluid Dynamic Viscosity

Superscripts

-	Averaged Value

Subscripts

air	Air
bulk	Local Bulk Temperature
DB	Value Predicted by Dittus-Boelter Correlation
h	Hydraulic
p	Constant Pressure
w	Wall

Abbreviations

AR	Aspect Ratio
CFD	Computational Fluid Dynamics
LES	Large Eddy Simulation
RANS	Reynolds-Averaged Navier-Stokes
TLC	Thermochromic Liquid Crystal

SUMMARY OF PRECEDING WORK

The current study was preceded by heat transfer and friction testing by Slabaugh et al. in [28, 29, 30]. The Nusselt number augmentation and friction factor augmentation of the channels studied are shown in Fig. 3. The results of those studies indicated that the double dimple feature had marked improvements over the single dimple design. When comparing the double dimple feature to the two different sized single dimple features, the double dimple was comparable to the advancement in heat transfer augmentation from the large dimple, with the lower frictional cost of the small dimple. A more detailed study on the unique performance of the double dimple geometry is the motivation for the current study in which an attempt is made to isolate the heat transfer within the dimple from the surrounding non-dimpled surfaces for better insight into the higher heat transfer promoted by the double dimple as well as the effect of the dimples on the surrounding smooth wall surfaces between the dimples.

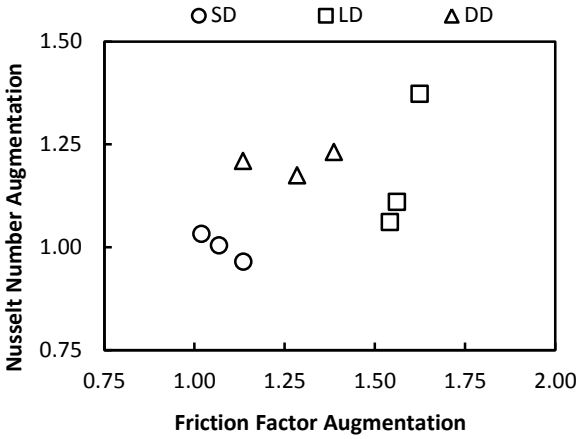

Figure 3: Overall Performance of SD, LD, and DD [28]

TEST SECTION

An overview of the present setup of this experiment is shown in Fig. 4. Flow is provided by a vortex blower operated under suction from air at ambient conditions. A gate valve controls the flow rate while a calibrated venturi is used to measure the flow rate. Tests are conducted at 10,000, 18,000, 27,000, and 36,000 channel averaged Reynolds number, based on hydraulic diameter of the smooth walled channel. The flow is considered incompressible, as the maximum Mach number is less than 0.2.

The heated test section is made up of ten segmented copper modules totaling a length of ~25 hydraulic diameters (based on the non-featured channel dimensions). Each module consists of 4 copper blocks: the bottom wall is featured and the top and side walls are smooth. An acrylic featured entrance section (~35 D_h) was used to ensure a hydrodynamically fully developed flow before entering the heated test section. Incoming air at the inlet of the entrance section is from ambient.

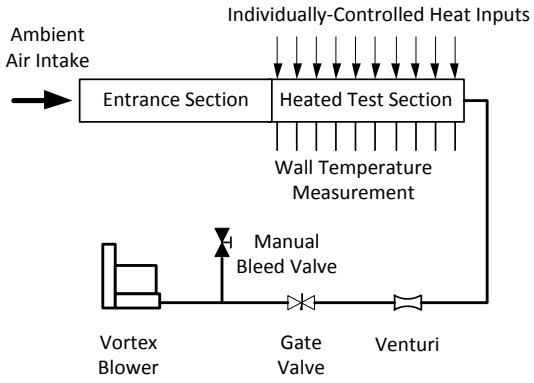

Figure 4: Current Experimental Setup

Three thermocouples are placed immediately at the inlet and exit of the heated test section to measure the inlet and exit bulk temperature.

The modules of the heated test section are depicted in Fig. 5. The four copper blocks are held within an acrylic housing to form a 2:1 AR channel. The acrylic housing is also meant to provide a structure that will allow the copper to form a channel without physical contact between the four blocks of each module to eliminate conduction between blocks of each module. To minimize conduction between adjacent blocks on each wall, the copper pieces are separated with cork insulation. The copper blocks contain two, for redundancy, T-type thermocouples inserted into machined holes in the back of the block, to measure wall temperature, held in place with high conductivity thermal cement. The thermocouple measurements are recorded using a Measurement Computing© data acquisition system.

Each copper block is backed by a thin foil heater, held to the block with double-sided Kapton™ tape. The heaters are manufactured to cover the surface of the copper block. Power is supplied to the heaters by a 300 Amp adjustable DC power source. The top, bottom, and side heaters are each controlled by an array of rheostats such that the voltage applied to each heater can be individually controlled. The voltage applied to each heater is measured with a digital multimeter.

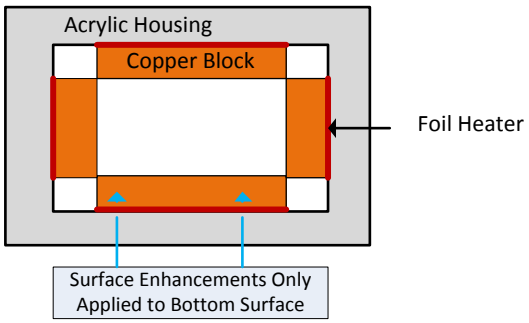

Figure 5: Cross-Section of Channel

GEOMETRIC FEATURES STUDIED

This experiment examines three types of dimples, a spherical small dimple, a spherical large dimple, and a double dimple geometry. Important non-dimensional parameters are listed in Table 1 with a figure of their description in Fig. 6. The small dimple feature is denoted as 'SD,' the large dimple as 'LD,' and the double dimple is denoted as 'DD.' The small dimple has a smaller dimple radius and depth whereas the large dimple has the largest dimple radius and dimple depth. The double dimple geometry is two small dimples incorporated into one compound feature. The upstream and downstream dimple of the double dimple are identical and both have an equal radius and depth to the small dimple that are offset in the streamwise position by 0.367d and aligned in the spanwise direction. The double dimple and small dimple arrays also have identical streamwise and spanwise pitch. The dimple density is also listed as a percentage of the projected flat area of the bottom wall covered by the dimple footprint.

Table 1: Geometric, Non-dimensional Dimple Parameters

Geometry	R/d	H/d	δ/d	P/d	S/d	Dimple Density
SD	**0.64**	**1.33**	**0.26**	**1.00**	**1.41**	**21%**
LD	**0.65**	**0.95**	**0.24**	**0.42**	**1.00**	**41%**
DD	**0.64**	**1.33**	**0.26**	**1.00**	**1.41**	**30%**

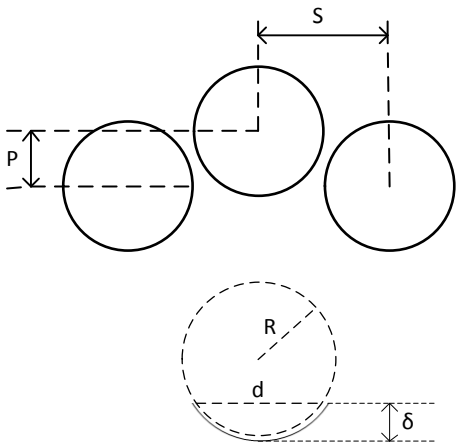

Figure 6: Description of Geometric Parameters

Selected blocks in the channel have been fitted with Rohacell (k=0.028W/m-K) dimpled features; the remaining blocks are entirely made of copper with a dimpled surface, as shown in Fig. 7. The dimple footprint was bored out to half the depth of the copper block and replaced with a Rohacell dimple insert to restore the geometry of the dimple feature.

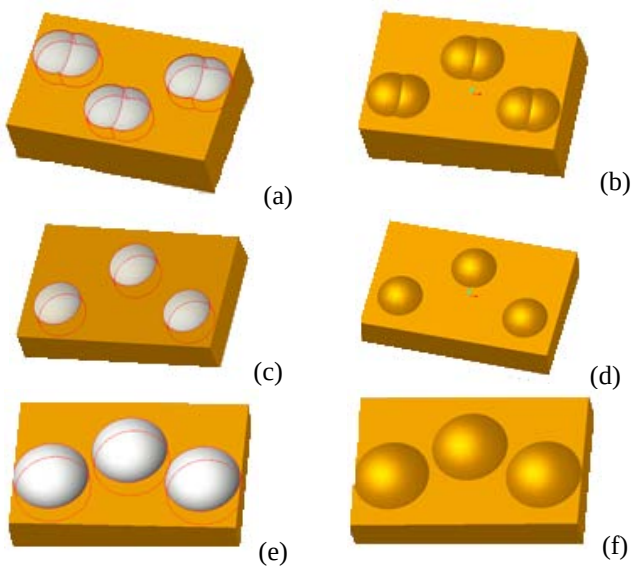

Figure 7: Featured Copper Block; (a) Rohacell Double Dimple, (b) Full Copper Double Dimple, (c) Rohacell Small Dimple, (d) Full Copper Small Dimple, (e) Rohacell Large Dimple, (f) Full Copper Large Dimple

A conservative estimate for the heat conduction through the Rohacell was performed and calculated as percentages of the total heat input (shown in Table 2). The estimate, performed numerically, using Gambit to mesh a single copper-block with Rohacell inserts and Fluent to solve the heat conduction equation, was completed by applying appropriate boundary conditions at all surfaces. Heat flux from the surface of the Rohacell dimple was then determined and compared with the overall heat input. This estimate was verified using T-type thermocouples implemented to measure the surface temperature of the Rohacell at multiple locations during testing. The actual measured surface temperatures resulted in a smaller percentage of heat loss than the conservative estimate performed. The heat transfer within the dimple (of the Rohacell blocks) is assumed to be zero in this study with the disclaimer that the interpreted results may be skewed and that the Nusselt number of the blocks with Rohacell inserts may be slightly overestimated.

Table 2: Rohacell Heat Loss Estimate

Geometry	Initial Estimate
SD	5%
LD	8%
DD	6%

HEAT TRANSFER TESTING PROCEDURE

A curve fit for the amount of heat lost to the surroundings and a curve fit for resistances for each heater are determined experimentally. The channel is filled with fiberglass insulation to reduce natural convection within the channel. Heat is supplied to the heaters to achieve a constant wall temperature, with no flow so that the effect of lateral conduction can be ignored. After the channel has reached steady state, the wall temperature of each block is recorded at 2 Hz for 1800 samples per thermocouple to reduce precision uncertainty. The voltage and resistance of each heater is also recorded. Three wall temperatures are tested to create the curve-fit equations.

From these recorded values, the amount of heat loss at each block is determined from Eq. (1).

$$Q_{loss} = \frac{V^2}{R(T_w)} = fn(T_w - T_{amb}) \quad (1)$$

A second order polynomial is curve fit to the amount of Q_{loss} versus the temperature difference ($\Delta T = T_w - T_{amb}$) with the constraint that the heat loss is zero when the ΔT is zero. A linear curve fit is performed on the resistance versus the wall temperature. These curve fit equations are then used in the data reduction.

To begin the heat transfer tests, first the flow rate is set to the desired Reynolds number. The flow rate is calculated by measuring the pressure drop across the venturi with a handheld digital manometer. The voltage applied to each heater is adjusted to achieve a constant wall temperature of ~70°C throughout the entire heated test section. After steady state is achieved, the wall temperatures of each module and voltages applied to each heater are recorded.

DATA REDUCTION

To determine the contribution of the flow within the dimple to the heat transferred from the surrounding surface, local heat transfer data is determined by first finding power generated by the foil heaters using Eq. (2):

$$Q_{input} = \frac{V^2}{R(T_w)} \tag{2}$$

V is measured for each heater during each test and R of each heater is calculated from the measured wall temperature and the resistance curve fit equation as mentioned earlier.

The actual heat input is then calculated as shown in Eq. (3). The Q_{loss} is determined from the wall temperature measured and the heat leakage curve fit equation determined as described above. Heat loss as a percent of Q_{input} ranges from 10-30%, depending on block location in the channel and Reynolds number tested.

$$Q_{actual} = Q_{input} - Q_{loss} + Q_{lateral} \tag{3}$$

$Q_{lateral}$ is calculated, using a 1D heat conduction model, where resistance is calculated in Eq. (4), and temperature difference is calculated for adjacent blocks. In Eq. (4), k_{cork} and $A_{contact}$ are the conductivity and contact area of the cork insulation between adjacent blocks. Maximum $Q_{lateral}$ percentage based on Q_{input} was 3%.

$$R_{lateral} = \frac{t}{k_{cork} * A_{contact}} \tag{4}$$

The bulk temperature at each location in the channel is calculated using a bulk temperature march starting from the inlet using an energy balance as described in Eq. (5):

$$T_{bulk_i} = T_{bulk_{i-1}} + \frac{Q_{added_i}}{\dot{m} * c_p} \tag{5}$$

The value of Q_{added}, is defined in Eq. (6) is the sum of the heat transferred to the flow from the second half of the preceding copper block and the first half of the copper block where the bulk temperature is being calculated, indicated by the drawing in Fig. 8.

$$Q_{added_i} = 0.5 * Q_{actual_{i-1}} + 0.5 * Q_{actual_i} \tag{6}$$

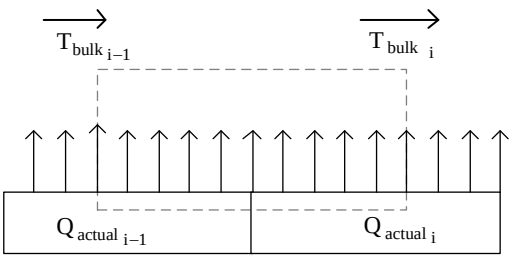

Figure 8: Calculation of T_{bulk}

All flow properties are evaluated at the local film temperature at each block Eq. (7):

$$T_{film} = \frac{T_{wall} + T_{bulk}}{2} \tag{7}$$

Knowing the bulk temperature throughout the flow and the power added to the flow at each point of temperature measurement, the heat transfer coefficient of each block can be calculated from Newton's Law of cooling, Eq (8):

$$Q = hA_{ref}(T_{wall} - T_{bulk}) \tag{8}$$

A_{ref} is the projected, participating heat transfer surface area, as denoted by the hashed marking in Fig. 9. Note that A_{ref} is less for copper blocks with Rohacell inserts; A_{ref} for these Rohacell insert blocks is the non-featured surface area, whereas A_{ref} for the full copper blocks is the projected surface area of the non-featured and featured surface.

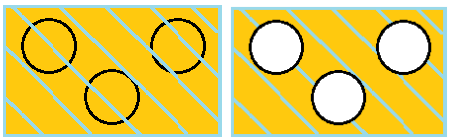

(a) (b)

Figure 9: Surface Area (a) "Bottom-A" Full-Copper Blocks (b) "Bottom-B" Copper with Rohacell Inserts

The Nusselt number is then determined from the heat transfer coefficient using the hydraulic diameter as the characteristic length, Eq (9).

$$Nu = \frac{h \cdot D_h}{k_{air}} \tag{9}$$

The Dittus-Boelter correlation for heat transfer in a smooth pipe, Eq. (10), is used for comparison of the Nusselt numbers obtained in this study; the 0.4 exponent on Pr is used for heating of the fluid.

$$Nu_{DB} = 0.023Re^{0.8}Pr^{0.4} \tag{10}$$

The overall channel averaged heat transfer augmentation is calculated using the area weighted average Nusselt number of each wall divided by the predicted Nusselt number from the Dittus-Boelter correlation.

UNCERTAINTY

The calculated experimental uncertainty for the overall heat transfer augmentation was performed using the procedures described by [31-33]. The uncertainties at each Reynolds number are shown in Table 3. Uncertainties per block were also calculated, error bars for blocks on the bottom wall are

displayed on the local Nusselt number data in the results. The additional uncertainty caused by the heat loss through the Rohacell dimple for the Rohacell blocks was ignored, but these blocks were not used in the calculation of the overall Nusselt number augmentation. The overall uncertainties for the channel Reynolds number were ±3.7% (with higher uncertainty being at lower Reynolds number).

Table 3: Uncertainty in Overall Nusselt Number Augmentation

Re	SD	LD	DD
10,000	± 3.6%	± 5.3%	± 7.7%
18,000	± 2.5%	± 5.8%	± 4.4%
27,000	± 3.9%	± 4.1%	± 5.2%
36,000	± 3.0%	± 2.9%	± 5.3%

BASELINE VALIDATION OF CURRENT SETUP

Validation of the experimental setup and procedure was performed prior to the dimpled wall experiment. Smooth wall copper blocks were implemented on the bottom wall using the same experimental setup and procedure. Overall Nusselt number results of this smooth wall baseline experiment were in agreement to the well-established correlations, within 1% of the Dittus-Boelter correlation and within 13% of the Gnielinski correlation for the each of the Reynolds numbers tested.

COMPARISON TO PREVIOUS RESULTS

A comparison to the previous study [28] for all three dimple geometries is shown in Figs. 10-12. The plot displays the average Nusselt numbers for each of the walls individually, where "Bottom-Current" averages only "Bottom-A," the full copper blocks. The 10,000 Reynolds number case was not performed in [28]. However, for the current study, the Nusselt number on each wall at the lowest Reynolds number follows the increasing trend of the three higher Reynolds numbers tested. For the large dimples, the Nusselt numbers on the bottom wall in the current study at the 18,000 Reynolds number are offset from the previous study. All other cases fall within the experimental uncertainty of each study. With the exception of the offset on the LD at 18,000 Reynolds number, the agreement with the previous work adds valuable confidence in the current results. A similar comparison of local Nusselt number trends show favorable matching between the full copper blocks.

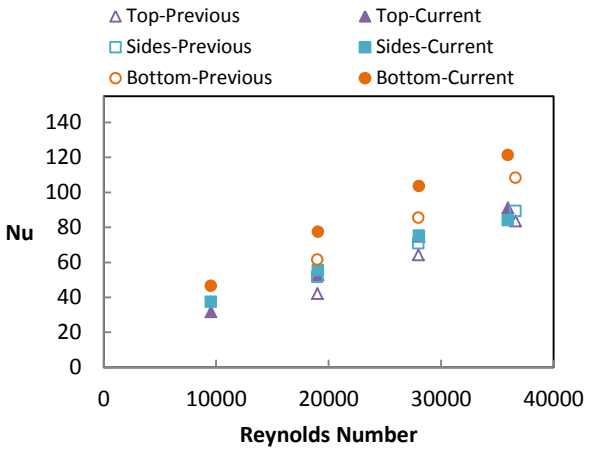

Figure 10: Comparison to [28] of Small Dimple

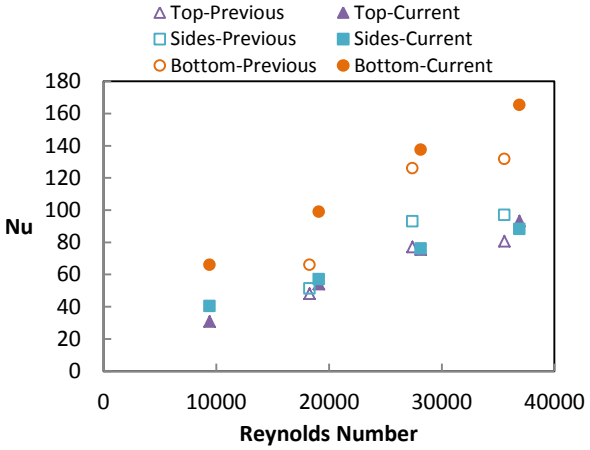

Figure 11: Comparison to [28] of Large Dimple

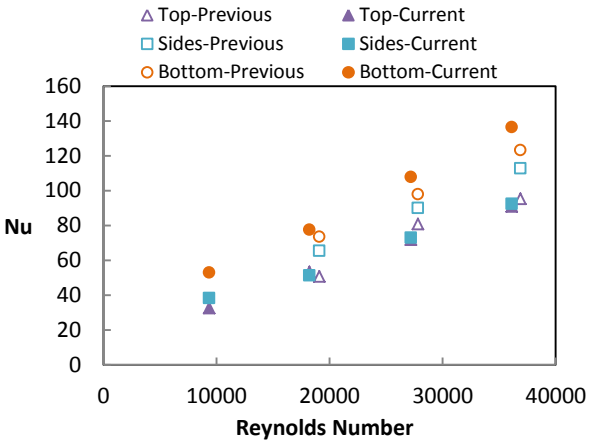

Figure 12: Comparison to [28] of Double Dimple

SMALL DIMPLE

The local Nusselt numbers of the first nine copper modules for the SD case are plotted against the streamwise position normalized by the hydraulic diameter for all four Reynolds numbers in Fig. 13. The 10th module is omitted because of exit

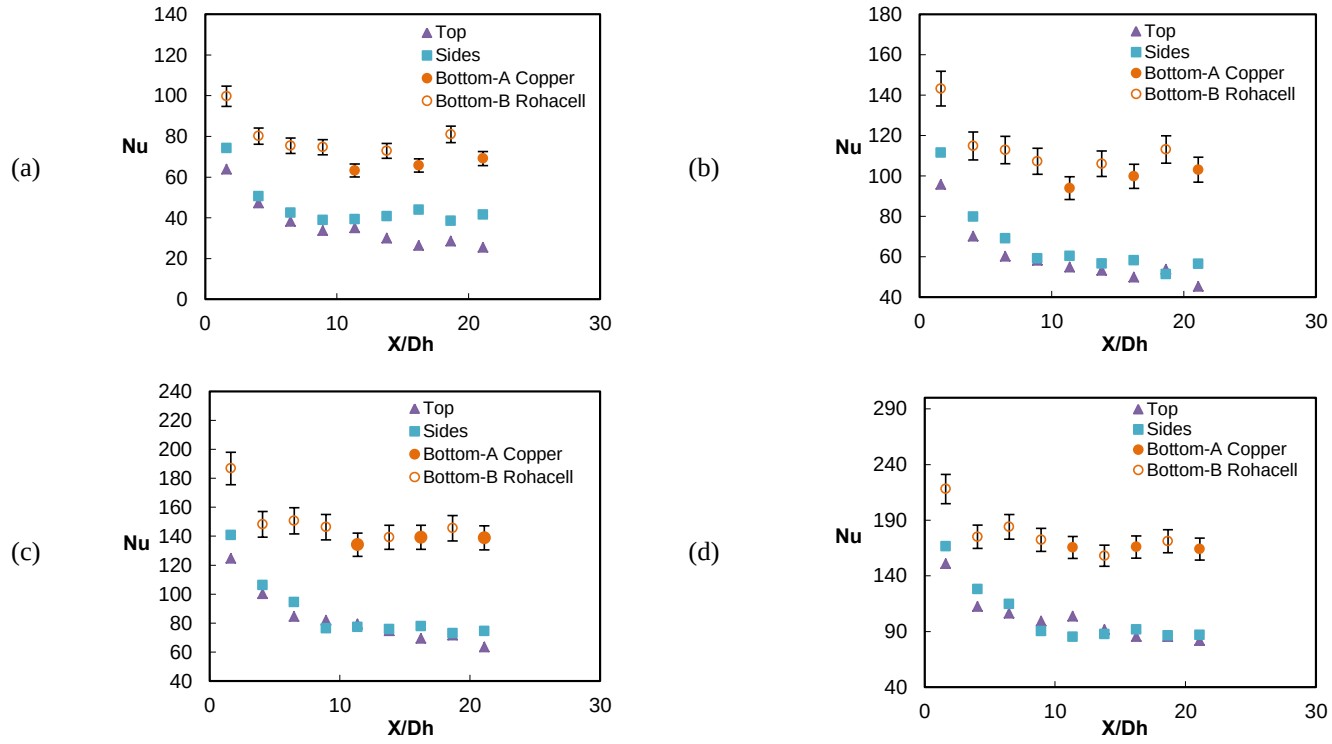

Figure 13: Local Nusselt Number for SD Channel (a) 10,000 Re (b) 18,000 Re (c) 27,000 Re (d) 36,000 Re

effects from the transition of the test channel to an exit pipe. For the bottom wall, the copper-only modules are denoted by 'Bottom-A' whereas the copper modules that were embedded with the Rohacell dimples are denoted by 'Bottom-B'. Although Bottom-A and Bottom-B blocks have identical features, when calculating the Nusselt numbers of the blocks, the dimple footprint area is subtracted from the projected surface area for Bottom-B, since the heat conducted through the Rohacell is neglected. By subtracting this area out, the Nusselt number values obtained for Bottom-B depict convection from the smooth surfaces outside of the dimples and capture only the effect the dimples have on the adjacent smooth surface on the bottom wall.

A summary of the wall-averaged and overall channel averaged Nusselt numbers and Nusselt number augmentations in the fully developed portion of the channel ($X/D_h > 10$) are shown in Table 4. A comparison is shown for the average Nusselt number and Nusselt number augmentation for all four walls. Average Nusselt number and Nusselt number augmentation is also shown for the overall channel. Only the Bottom – A modules are used to calculate the overall channel (area-weighted average) Nusselt number since the Bottom – B modules are not representative of the heat transfer of the entire bottom wall. However, the Nusselt numbers of the Bottom-B modules do provide useful insight since they capture the impact of the secondary flows created by the dimples on the non-dimpled portion of the bottom wall.

It is found that the Nusselt numbers of the B blocks are greater than the A blocks at low Reynolds number and comparable at higher Reynolds numbers. The heat transfer augmentation on the non-featured portion of the bottom wall can be inferred to exceed that of the augmentation within the dimple, based on the offset between Nusselt number for Bottom-A and Bottom-B. At the higher Reynolds numbers, where the difference between the heat transfer augmentation between Bottom-A and Bottom-B is minimal, the heat transfer within the dimples can be considered comparable to the heat transfer on the adjacent smooth walls. These findings show that dimples are capable of promoting heat transfer on the entire bottom wall; the effects are not confined to just within the dimple, consistent with findings presented in previous studies including Mahmood et al. [9], Burgess and Ligrani [14], and Borisov et al. [20].

On the non-featured portions of the bottom wall, the heat transfer enhancement occurs by the ejection of vortices from the dimple as well as the secondary flows induced by the dimple. On the other hand, the heat transfer enhancement within the dimple cavity occurs through a different mechanism, as reviewed in previous literature [9,14]. Flow separation occurs as the flow passes over the cavity; a large recirculation zone occupies the upstream region of the dimple resulting in relatively poor heat transfer. Downstream of the separation zone, the flow reattachment on the trailing edge surface of the dimple improves heat transfer because of the impingement. The recirculation can occupy a large portion of the dimple, which helps to explain why the heat transfer enhancement on the non-dimpled portion of the bottom wall can receive significant enhancement (Bottom-A ≤ Bottom-B); the high heat

transfer of the flow reattachment is partially negated by the recirculation where there is relatively poor heat transfer (see Fig. 2a).

In this narrow channel study, the dimples are being confined by the side and top walls. This confinement is severe, compared with previous studies where large dimple arrays are used. The benefit on the top and side walls from the dimple is not seen at the three higher Reynolds numbers, with a heat transfer augmentation near unity. Although no benefit on the top and side walls is observed here, the side and top walls may be influencing the heat transfer on the bottom wall. The degree of this effect cannot be fully evaluated in the present study, and requires a more detailed study. In highly turbulent flows, for the three higher Reynolds numbers, the surface feature has less effect on the heat transfer of the surrounding smooth walls. At the 10,000 Reynolds number, the heat transfer augmentation of the side walls is significantly improved. Looking at a vast dimple array with previous studies, rather than the confined channel studied, would have neglected these effects on side walls that exist in the compact heat exchanger or microchannel design. The addition of dimples to the bottom wall contributed to an increase of ~20% improvement on the side walls. However, no additional augmentation on the top wall is observed. The improved performance of the side walls at the low Reynolds number is likely a result of more efficient flow interactions between the dimples and surrounding walls. There may be additional flow interactions taking place because the flow disturbance induced by the dimple is confined by the presence of nearby walls as a result of the low aspect ratio of the channel. These dimple-wall interactions would not occur in the high aspect ratio channels or dimple arrays as studied by [21,25,26] and they would be less significant or weakened at high Reynolds numbers.

Even though the Nusselt number increases with Reynolds number, the overall heat transfer augmentation decreases with increasing Reynolds number, expectedly. As the flow becomes more turbulent, the flow interactions between the vortices ejected out of the dimple and the turbulent free-stream flow are less significant because of the increased free-stream turbulence, diminishing the effect the dimpled features have on the heat transfer augmentation. The decrease of heat transfer augmentation with increasing Reynolds number is typical of internal cooling channels and is consistent with similar results of Burgess and Ligrani, discussing stronger secondary flows and vortices produced by the dimples at lower Reynolds numbers and some suppression of secondary flows and vortices at higher Reynolds numbers [14,15].

Consistency of Nusselt number augmentation at higher Reynolds numbers for dimples makes them useful over a wide range of flow rates, but also makes the mechanism of heat transfer of dimples difficult to assess and has plagued experimental researchers in this field. The ambiguity of dimples makes them both useful and difficult to understand. On the other hand, the similar Nusselt number ratios at high Reynolds numbers means that the dominant heat transfer mechanism for those cases is similar. The difference exists in going to a low Reynolds number, where the trends change (overall and sidewall enhancement at 10,000 Re), which indicates that the mode of heat transfer enhancement is different for the 10,000 Reynolds number than the three higher Reynolds numbers. There is possibly an onset of new flow phenomena at low Reynolds numbers that calls for further investigation.

Table 4: Averaged Nusselt Number and Nusselt Number Augmentation of SD

Small Dimple					
Re	Wall	Nu	Nu/NuDB	Nu (overall)	Nu/NuDB (overall)
10,000	Top	32	1.04	39	1.27
	Sides	37	1.23		
	Bottom - A	47	1.53		
	Bottom - B	52	1.70		
19,000	Top	53	1.00	62	1.17
	Sides	56	1.05		
	Bottom - A	77	1.46		
	Bottom - B	81	1.53		
28,000	Top	75	1.03	85	1.17
	Sides	75	1.04		
	Bottom - A	104	1.43		
	Bottom - B	106	1.47		
36,000	Top	91	1.03	100	1.13
	Sides	84	0.95		
	Bottom - A	121	1.38		
	Bottom - B	123	1.40		

Table 5: Averaged Nusselt Number and Nusselt Number Augmentation of LD

Large Dimple					
Re	Wall	Nu	Nu/NuDB	Nu (overall)	Nu/NuDB (overall)
10,000	Top	31	1.02	47	1.54
	Sides	40	1.34		
	Bottom - A	66	2.19		
	Bottom - B	77	2.56		
18,000	Top	54	1.01	70	1.32
	Sides	57	1.08		
	Bottom - A	99	1.86		
	Bottom - B	109	2.05		
27,000	Top	75	1.04	96	1.33
	Sides	76	1.05		
	Bottom - A	137	1.90		
	Bottom - B	144	1.98		
36,000	Top	93	1.04	120	1.33
	Sides	88	0.98		
	Bottom - A	165	1.84		
	Bottom - B	167	1.86		

LARGE DIMPLE

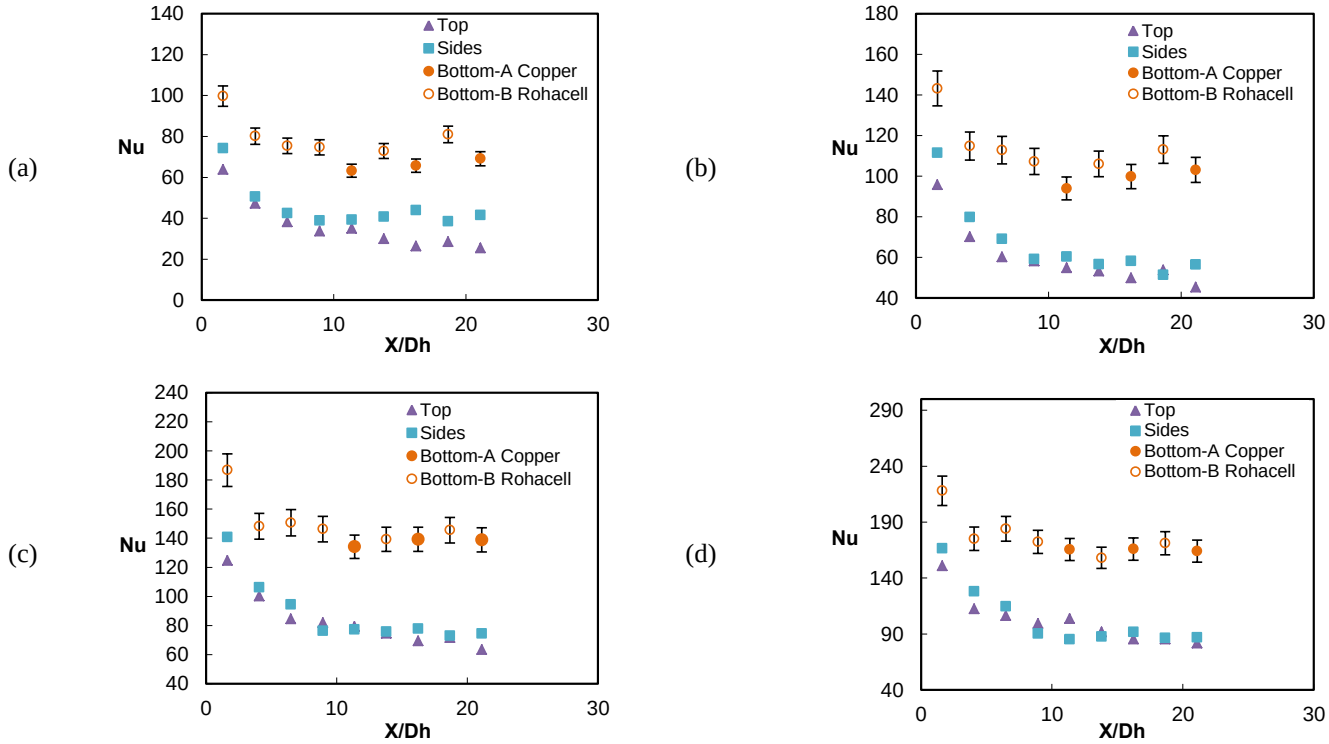

Figure 14: Local Nusselt Number for LD Channel (a) 10,000 Re (b) 18,000 Re (c) 27,000 Re (d) 36,000 Re

The local Nusselt numbers of each copper module for the LD case is plotted against the streamwise position normalized by the hydraulic diameter, in Fig. 14; the calculated averaged quantities are reported in Table 5.

The trends for the LD case are similar to those of the SD case. For the three lower Reynolds numbers tested, the heat transfer augmentation was greater on Bottom – B than Bottom – A, with augmentations equivalent at the highest flow rate. This result is supported by the discussion in the SD section; the heat transfer within the dimple feature contributes less to the overall augmentation than the adjacent smooth surfaces on the bottom wall at the lower Reynolds numbers, with comparable augmentation at 36,000.

Similar to the SD case, no contribution to the top and side walls from the large dimple is observed at the three higher Reynolds numbers for the LD; the heat transfer augmentation of the top and side walls are near unity for the 18,000, 27,000, and 36,000 Reynolds numbers. A 30% improvement in heat transfer augmentation on the side wall at 10,000 Reynolds number is observed on the LD, with no improvement on the top wall.

The overall heat transfer augmentation remains constant for the three higher Reynolds numbers, decreased from the 10,000 Reynolds number case. The similar overall Nusselt number ratios at all three higher Reynolds numbers is useful for applications that need consistent heat transfer augmentation over a range of flow rates.

DOUBLE DIMPLE

The local Nusselt numbers of each copper module for the DD case are plotted for in Fig. 15; the averaged quantities are reported in Table 6.

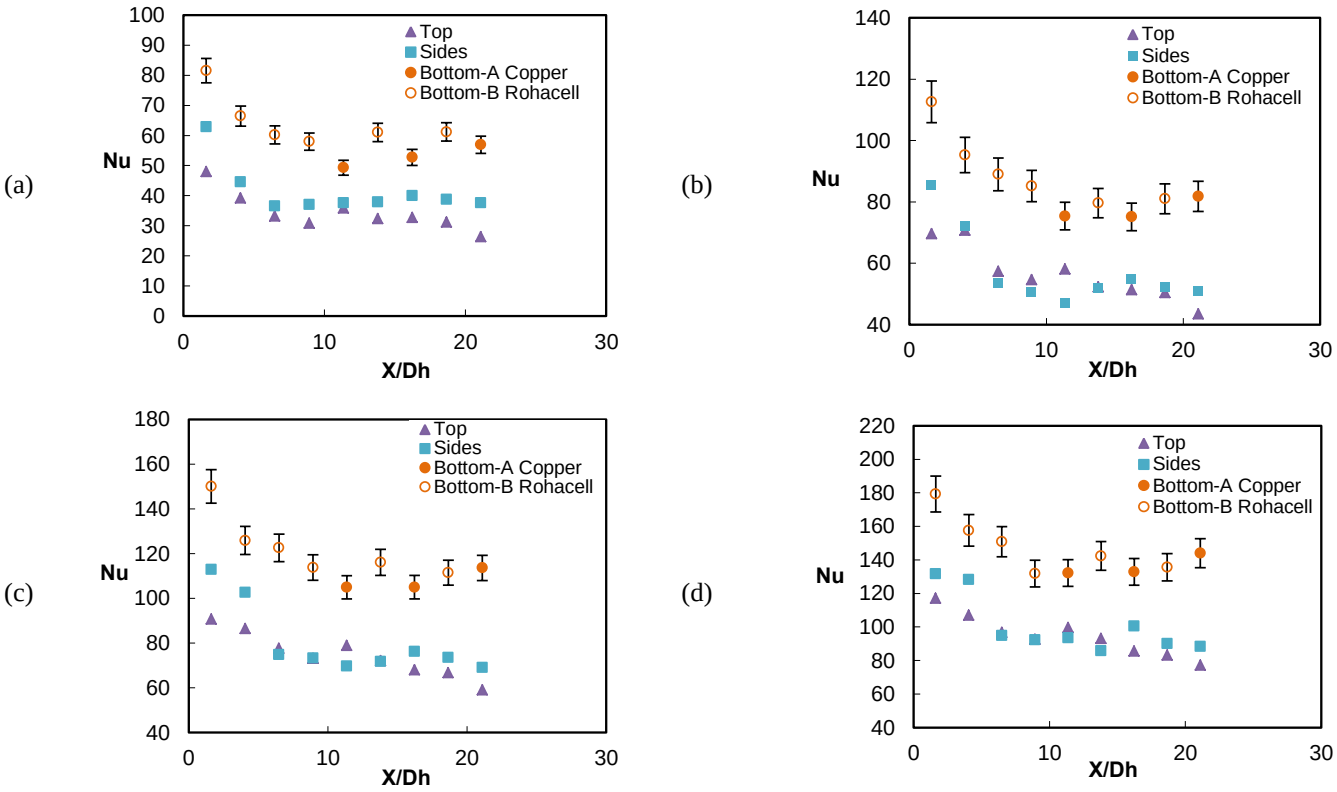

Figure 15: Local Nusselt Number for DD Channel (a) 10,000 Re (b) 18,000 Re (c) 27,000 Re (d) 36,000 Re

The trends for the DD case are similar to those of the SD and LD case. Again, the difference in Nusselt numbers between Bottom – B and Bottom – A decreases as the Reynolds number increases. For the 10,000, 18,000, and 27,000 cases, the Bottom – B Nusselt number exceeds the Nusselt number on Bottom – A. This recurring trend supports the discussion in the SD and LD sections; the heat transfer within the double dimple feature contributes less to the overall augmentation than the adjacent smooth surfaces on the bottom wall at lower Reynolds numbers and contributes to a comparable amount at higher Reynolds numbers.

Again, there is no contribution to the top and side walls from the double dimple at the three higher Reynolds numbers; the heat transfer augmentation of the top and side walls are near unity for the 18,000, 27,000, and 36,000 Reynolds numbers for the double dimple case. A 20% improvement in heat transfer augmentation on the side wall at 10,000 Reynolds number is observed on the DD, as observed with the SD and LD case. A minor effect from the double dimple geometry onto heat transfer augmentation at the top wall for 10,000 Reynolds number is observed, approximately 9% with 5% uncertainty from Table 3. The improved performance of the top and side walls at low Reynolds number again is likely a result of more efficient flow interactions between the double dimples and surrounding walls.

The overall heat transfer augmentation, as seen with the LD, remains constant for the three higher Reynolds numbers and is decreased from the 10,000 Reynolds number case.

Table 6: Averaged Nusselt Number and Nusselt Number Augmentation of DD

Double Dimple					
Re	Wall	Nu	Nu/NuDB	Nu (overall)	Nu/NuDB (overall)
10,000	Top	33	1.09	42	1.39
	Sides	38	1.27		
	Bottom - A	53	1.76		
	Bottom - B	66	2.20		
18,000	Top	53	1.04	61	1.18
	Sides	51	1.00		
	Bottom - A	77	1.51		
	Bottom - B	82	1.60		
27,000	Top	72	1.02	84	1.19
	Sides	73	1.03		
	Bottom - A	108	1.53		
	Bottom - B	114	1.62		
36,000	Top	91	1.03	108	1.22
	Sides	92	1.05		
	Bottom - A	136	1.55		
	Bottom - B	137	1.55		

CONCLUSION

The heat transfer augmentation of a small dimple, large dimple, and double dimple channel was investigated at channel Reynolds numbers of 10,000, 18,000, 27,000, and 36,000. As the Reynolds number increased, the overall heat transfer enhancement decreased for all three geometries tested, because of the increased free-stream turbulence with increasing Reynolds number.

Interactions occurring between the dimple-induced secondary flows and the side walls resulted in an increase in heat transfer augmentation at the 10,000 Reynolds number case for all three geometries. An increase in heat transfer augmentation on the top wall at this flow rate was also observed for only the double dimple. The side walls of both the double dimple and small dimple had similar heat transfer augmentations at this flow rate (~20%), where the large dimple side wall heat transfer augmentation at 10,000 Reynolds number was higher (~30%). Heat transfer on the top wall was improved by ~10% in the double dimple case.

For the bottom featured wall, the heat transfer augmentation of Bottom – B was greater than Bottom – A for all three geometries at the 10,000, 18,000, and 27,000 Reynolds numbers. At the 36,000 Reynolds number, the difference between augmentation between Bottom – A and Bottom – B was minimal; there was no difference observed between the full copper and Rohacell insert blocks in heat transfer augmentation. The heat transfer augmentation on the adjacent smooth surfaces on the bottom featured wall, the insulated dimple blocks, contribute more to the overall augmentation than the full copper dimpled blocks at the lower Reynolds numbers tested and have similar contribution at higher Reynolds numbers. Results for each dimple geometry show that dimples are capable of promoting heat transfer over the entire bottom wall, the effects are not confined to just within the dimple cavity.

With this knowledge, additional research into the dimple density and dimple spacing parameters is needed before a completely optimized cooling channel can be realized. Further research is also necessary to characterize the impact of these flow disturbances to the smooth side and top walls. It can be added to the aforementioned that the flow field and heat transfer in a double dimpled channel as well as within the dimple cavity, particularly the double dimple, deserves further investigation.

ACKNOWLEDGMENTS

The authors acknowledge the support from the Florida Center for Advanced Aero Propulsion (FCAAP). This work was performed at and with the support from students and staff of the Siemens Energy Center - a research laboratory at the University of Central Florida made possible through funds from Siemens Energy.

REFERENCES

1. Snedeker, R. S., and Donaldson, C. D., 1966, "Observation of Bistable Flow in a Hemispherical Cavity," AIAA Journal, **4**(4) , pp. 735-736.

2. Murzin, V. N., Stoklitskii, S. A., and Chebotarev, A., 1986, "Creation of Solitary Vortices in a Flow Around Shallow Spherical Depression," Soviet Technical Physical Letters, **12**, pp. 547-548.

3. Belen'kiy, M. Y., Gotovskiy, M. A., Lekakh, B. M., Fokin, B. S., and Dolgushin, K. S., 1994, "Heat Transfer Augmentation Using Surfaces Formed by a System of Spherical Cavities," Heat Transfer-Sov. Res., **25**(2), pp. 196-203.

4. Terekhov, V. I., Kalinina, S. V. and Mshvidobadze, Y.M., 1995, "Flow Structure and Heat Transfer on a Surface with a Unit Hole Depression," Russ. J. Eng. Thermophys, **5**, pp. 11–34.

5. Chyu, M. K., Yu, Y., Ding, H., Downs, J. P., and Soechting, F. O., 1997, "Concavity Enhanced Heat Transfer in an Internal Cooling Passage," ASME 42nd International Gas Turbine and Aeroengine Congress and Exposition, Orlando, FL.

6. Moon, S. W., and Lau, S. C., 2002, "Turbulent Heat Transfer Measurements on a Wall with Concave and Cylindrical Dimples in a Square Channel," GT-2002-30208, Proc. ASME Turbo Expo 2002, Amsterdam, The Netherlands.

7. Chyu, M. K., Yu, Y., Ding, H., 1999, "Heat Transfer Enhancement in Rectangular Channels with Concavities" Enhanced Heat Transfer, **6**(6), pp. 429-439.

8. Moon, H. K., O'Connell, T., Glezer, B., (2000) "Channel Height Effect on Heat Transfer and Friction in a Dimpled Passage," Journal of Engineering for Gas Turbines and Power, **122**(2), pp. 307-313.

9. Mahmood, G. I., Hill, M. L., Nelson, D. L., Ligrani, P. M., Moon, H. K., and Glezer, B., 2001, "Local Heat Transfer and Flow Structure on and Above a Dimpled Surface in a Channel," J. of Turbomachinery, **123**(1), pp. 115-123.

10. Mahmood, G. I. and Ligrani, P. M., 2002, "Heat Transfer in a Dimpled Channel: Combined Influences of Aspect Ratio, Temperature Ratio, Reynolds Number, and Flow Structure," International Journal of Heat and Mass Transfer," **45**(10), pp. 2011-2020.

11. Ligrani, P. M., Burgess, N. K., and Won, S. Y., 2005, "Nusselt Numbers and Flow Structure on and Above a Shallow Dimpled Surface Within a Channel Including Effects of Inlet Turbulence Intensity Level," J. Turbomachinery, **127**(2), pp. 321-330.

12. Won, S. Y., Zhang, Q., and Ligrani, P. M., 2005, "Comparisons of Flow Structure Above Dimpled Surfaces with Different Dimple Depths in a Channel," Physics of Fluids, **17**, 045105.

13. Burgess, N. K., Oliveira, M. M., and Ligrani, P. M., 2003, "Nusselt Number Behavior on Deep Dimpled Surfaces Within a Channel," J. Heat Transfer. **125**(1), pp 11-18.

14. Burgess, N.K., and Ligrani, P.M., 2004, "Effects of Dimple Depth on Nusselt Numbers and Friction Factors for Internal Cooling in a Channel," GT 2004-54232, Proc. ASME Turbo Expo, Vienna, Austria.

15. Burgess, N. K., and Ligrani, P. M., 2005, "Effects of Dimple Depth on Nusselt Numbers and Friction Factors," J. Heat Transfer. **127**(8), pp 839-847.

16. Isaev, S. A., Leontiev, A. I., Kudryatsev, N. A., and Pyshnyi, I. A., 2003, "The Effect of Rearrangement of the Vortex Structure on Heat Transfer under Conditions of Increasing Depth of a Spherical Dimple on the Wall of a Narrow Channel," High Temperature, **41**(2), pp. 229-232.

17. Griffith, T. S., Al Hadhrami, L., and Han, J.-C., 2003, "Heat Transfer in Rotating Rectangular Cooling Channels (AR=4) With Dimples," J. Turbomachinery, **125**(3), pp. 555-564.

18. Zhao, J. B., Chew, Y. T., and Khoo, B. C., 2004, "Experiemental Studies on Hydrodynamic Resistance and Flow Pattern of a Narrow Flow Channel with Dimples on the Wall," IMECE2004-59506, Proc. ASME International Mechanical Engineering Congress and Exhibition, Anaheim, CA, USA.

19. Borisov, I., Khalatov, A., Kobzar, S., & Glezer, B., 2004, "Comparison of Thermo-Hydraulic Characteristics for Two Types of Dimpled Surfaces," GT2004-54204, Proc. ASME Turbo Expo 2004, Vienna, Austria.

20. Borisov, I., Khalatov, A., Kobzar S., Glezer, B.**,** 2006, "Heat Transfer and Pressure Losses in a Narrow Dimpled Channel Structured with Spherical Protrusions," GT2006-90121, Proc. ASME Turbo Expo 2006, Barcelona, Spain.

21. Hwang, S. D., Kwon, H. G., and Cho, H. H., 2010, "Local Heat Transfer and Thermal Performance on Periodically Dimple-Protrusion Patterned Walls for Compact Heat Exchangers," Journal of Energy, **25**(12), pp. 5357-5367.

22. Leinhart, H., Breuer, M., and Koksoy, C., 2008, "Drag Reduction By Dimples? - A Complementary Experimental/ Numerical Investigation," International Journal of Heat and Fluid Flow, **29**(3), pp. 783-791.

23. Isaev, S. A., Kornev, N. V., Leontiev, A. I., and Hassel, E., 2010, "Influence of the Reynolds Number and the Spherical Dimple Depth on Turbulent Heat Transfer and Hydraulic Loss in a Narrow Vhannel," Int. J. of Heat and Mass Transfer, **53**, 178-197.

24. Leontiev, A. I., Isaev, S. A., Kornev, N. V., Chudnovsky, Y., and Hassel, E., 2010, "Numerical Modeling and Physical Simulation of Vortex Heat Transfer Enhancement Mechanisms over Dimpled Reliefs," IHTC14-22334, Proc. 14th International Heat Transfer Confernce, Washington, DC, USA .

25. Elyyan, M. A., Rozati, A., and Tafti, D. K., 2008, "Investigation of Dimpled Fins for Heat Transfer Enhancement in Compact Heat Exchangers," Int. J. Heat and Mass Transfer, **51**(11-12), pp. 2950-2966.

26. Elyyan, M. A., and Tafti, D. K., 2009, "A novel split-dimple interrupted fin configuration for heat transfer augmentation," Int. J. Heat and Mass Transfer, **52**(5-6), pp 1561-1572.

27. Carman, B. G., Kapat, J. S., Chow, L. C., and An, L., 2002, "Impact of a Ceramic Microchannel Heat Exchanger on a Micro Turbine," GT2002-30544, Proc. ASME Turbo Expo 2002, Amsterdam, The Netherlands.

28. Slabaugh, C. D, Tran, L. V., Ricklick, M., and Kapat, J. S., 2009 "A Study of Side Wall Heat Transfer Augmentation in a Narrow Rectangular Channel Duct," AIAA-2009-5377, Proc. 45th AIAA Joint Propulsion Conference, Denver, CO USA.

29. Slabaugh, C. D, Tran, L. V., Ricklick, M., and Kapat, J. S., 2010, "Side Wall Heat Transfer Augmentation in a Narrow Rectangular Channel with Dimples Applied to the Bottom Wall," AIAA-2010-6953, Proc. 46th AIAA Joint Propulsion Conference, Nashville, TN USA.

30. Slabaugh, C. D., 2010, "Heat Transfer and Friction Augmentation in a Narrow Rectangular Duct with Dimples Applied to a Single Wall," University of Central Florida, Orlando, FL USA.

31. PTC 19.1., 2005, Measurement uncertainty**,** ANSI/ASME Power Test Codes, American Society of Mechanical Engineers, New York.

32. Kline, S.J., McClintock, F.A., 1953, "Describing Uncertainties in Single Sample Experiments," Mechanical Engineering, **7**.

33. Moffat, R.J., 1985, "Uncertainty Analysis in the Planning of an Experiment," Journal of Fluids Engineering, 107, pp. 173-181.

